

Lab on a Chip

Accepted Manuscript



This is an *Accepted Manuscript*, which has been through the Royal Society of Chemistry peer review process and has been accepted for publication.

Accepted Manuscripts are published online shortly after acceptance, before technical editing, formatting and proof reading. Using this free service, authors can make their results available to the community, in citable form, before we publish the edited article. We will replace this *Accepted Manuscript* with the edited and formatted *Advance Article* as soon as it is available.

You can find more information about *Accepted Manuscripts* in the [Information for Authors](#).

Please note that technical editing may introduce minor changes to the text and/or graphics, which may alter content. The journal's standard [Terms & Conditions](#) and the [Ethical guidelines](#) still apply. In no event shall the Royal Society of Chemistry be held responsible for any errors or omissions in this *Accepted Manuscript* or any consequences arising from the use of any information it contains.

DNA separation and enrichment using electrohydrodynamic bidirectional flows in viscoelastic liquids

Hubert Ranchon^{1,2}, Rémi Malbec^{1,2}, Vincent Picot³, Audrey Boutonnet³, Pattamon Terrapanich^{1,2}, Pierre Joseph^{1,2}, Thierry Leïchlé^{1,2}, Aurélien Bancaud^{1,2}

¹ CNRS, LAAS, 7 avenue du colonel Roche, F-31400 Toulouse, France

² Univ de Toulouse, LAAS, F-31400 Toulouse, France

³ Picometrics Technologies, 478 rue de la Découverte, Miniparc Bât 1, 31670 Labège, France

Correspondence: abancaud@laas.fr

Keywords: DNA separation, DNA enrichment, microfluidics, capillary electrophoresis, counter flow, viscoelasticity

Abstract

DNA size separation followed by purification and enrichment constitute essential operations for genetic engineering. These processes are mostly carried out using DNA electrophoresis in gels or in polymer solutions, a well-established yet lengthy technique which has been notably improved using Lab-on-Chip technologies. So far innovations for DNA separation or enrichment have been mostly undertaken separately, and we present an approach that allows us to perform these two processes simultaneously for DNA fragments spanning 0.2–50 kilo base pairs (kbp) in length. Our technology involves an electric field and a counter hydrodynamic flow in viscoelastic liquids, in which we show the occurrence of transverse forces oriented toward the walls. These forces increase with DNA molecular weight (MW) and hence induce a progressive reduction in DNA migration speed that triggers size separation in microfluidic channels as well as in capillaries. The separation of MW markers in the range 1-50 kbp is achieved in 15 minutes, thus outperforming gel electrophoresis that takes ~3 hours for this sample. Furthermore the use of a funnel, where electric and flow fields are modulated spatially, enables us to adjust transverse forces so as to stall the motion of DNA molecules at a position where they accumulate at factors of up to 1000 per minute. In this configuration, we establish that the operations of DNA enrichment and separation can be carried out simultaneously for the bands of a DNA MW marker between 0.2-1.5 kbp diluted at 0.02 ng/ μ L in 30 s. Altogether our technology, which can readily be integrated as an in-line module in Lab-on-Chips, offers unique opportunities for sample preparation and analysis of minute genomic samples.

Introduction

Electrophoretic separation of DNA is a key process of molecular biology, which is used both for preparative and analytical operations. DNA electrophoretic mobility is essentially constant with the size of the molecule in bulk, requiring the use of separation matrices to obtain size-dependent transport properties¹. Separation matrices can be constituted of polymer solutions/gels or regular arrays of micro or nano-posts etched in glass or silicon². The development of nanostructures for DNA analysis has constituted a mainstream research orientation for Lab-on-Chip technologies³, and these researches resulted in good separation performances with continuous⁴ or pulsed fields⁵. This success also stimulated the development of novel strategies, including among others “entropic trapping”⁶, in which the matrix consists of consecutive deep and shallow trenches etched in silicon that form entropic energy barriers crossed more rapidly by longer chains. These technologies however did not prove to be sufficiently robust for their adoption by the molecular biology community, and the standard system for high-performance DNA analysis consists of capillaries of ~100 μm in diameter filled with concentrated polymer solutions⁷. The super-low dispersion of capillary electrophoresis, which is sufficient to reach single base resolution⁷, has played a key role for sequencing technologies⁸.

Efforts have been concomitantly devoted to the development of matrix-free separation technologies. Cyclic hydrodynamic and electrophoretic actuation has been shown to induce DNA radial migration towards the walls of capillaries⁹. Due to the dependence in DNA size of transverse migration forces, it has been suggested that this approach was relevant for separation. In fact, improved separation performances have been reported using continuous hydrodynamic flow actuation in confined capillaries of ~5 μm ^{10,11}. This strategy turned out to be reminiscent of hydrodynamic chromatography¹², in which separation is triggered by steric constraints that repel large molecule from the walls where the flow velocity is faster. Whether steric repulsion or radial migration is invoked, the mechanism of matrix-free separation relies on concentration modulations in the channel cross section. Interestingly concentration variations of spherical tracers^{13,14} and DNA¹⁵ could also be detected using viscoelastic fluids flowing in microchannels¹⁶. Particles accumulate toward the centerline due to transverse viscoelastic forces, which have been characterized both experimentally and theoretically^{17,18}. Using numerical analysis for a particle fixed in place by an additional force field, Lee and co-workers noted that (i) cross stream forces could be oriented toward the walls, and (ii) the amplitude of the resulting transverse force would be much higher than for a freely suspended particle¹⁹. We reasoned that this conjecture could be tested experimentally using electrophoresis continuously acting opposite to the flow direction in order to stall the motion of charged solutes, and hence generate transverse viscoelastic forces oriented toward the walls. Using

single particle tracking of nanoparticles or λ -DNA molecules of 50 kbp, we demonstrate that the combination of hydrodynamic and electrophoretic actuations provides an efficient solution to monitor the amplitude of viscoelastic forces. We then establish the conditions for high performance DNA separation in microfluidic chips as well as in capillaries with this technology. We finally show that the operations of DNA enrichment and separation can be carried out simultaneously using the spatial modulations of the flow and the electric field in a microfluidic funnel. The overall performances of our technology, as characterized by the concentration enrichment factor of $\sim 10^3$ per minute and the separation of a molecular weight DNA marker including fragments ranging from 1 to 48.5 kbp in less than 17 minutes, offer a versatile toolbox for DNA analysis in Lab-on-Chips.

Experimental regime

The viscoelastic fluid was composed of a low conductivity buffer for electrophoresis (2X TBE, see methods) supplemented with variable proportions of poly-vinylpyrrolidone (PVP, 360 kDa) spanning 0.1-5% (m:v) filtered at 0.2 μm . PVP was used for its coating properties, which reduce the strength of electroosmotic flow ²⁰, as well as its viscoelastic properties above the entanglement threshold of $\sim 0.7\%$ ^{21,22}. The concentration of PVP was set to 2% in most experiments. The corresponding viscosity and elastic relaxation time were $\eta \sim 5.5$ mPa.s and $\lambda \sim 15$ ms, respectively (Supplementary Figure S1).

We used silicon chips of $h=2-10$ μm and $w=200$ μm in height and width, respectively (see details of the fabrication in ref. ²³), or glass capillaries of inner diameter $D \sim 10-75$ μm (Figure 1A). The length L of the separation channel was 0.5 and 12 cm for microfluidic chips and capillaries, respectively. The electric field E was tuned in the range 0.2-5 kV/m, and the maximum flow velocity v_0 spanned 100-3000 $\mu\text{m/s}$. Inertial forces were negligible because the Reynolds number was in the range of $10^{-5}-10^{-2}$. The Deborah number De , which measures the product of the fluid relaxation time by the shear rate $\dot{\gamma} \sim v_0/h \sim 30-300$ s^{-1} , was $\sim 0.5-5$, implying that the elasticity of the fluid had to be considered to describe the transport of DNA or particles ²⁴.

Qualitative model of cross stream viscoelastic forces

We propose to qualitatively describe the physics of cross stream migration acting on particles or DNA in the context of electrohydrodynamic actuation. We start from the argument of Leshansky and collaborators ¹³, which postulates that the transverse viscoelastic force is determined by the normal stress difference $N_I = \sigma_{zz} - \sigma_{xx}$ (see Figure 1A for geometry) For a Maxwell fluid, such as a solution of PVP ¹⁶, N_I is expected to scale with the square of the shear rate, as defined by $\dot{\gamma} \sim \partial v_x / \partial z$. The physical basis of this model is that shearing of the fluid leads to an excess of elastic stress

stored by the polymer around a particle, which in turn induces lateral movements toward regions with minimal shearing so as to reduce the elastic energetic penalty.

We then propose to evaluate the spatial dependence of the viscoelastic force by finite element modeling. We consider a charged bead of 100 nm in diameter transported in a microchannel of $h=4\ \mu\text{m}$ (Figure 1). We assume that the effective velocity of a particle is defined as the sum of hydrodynamic and electrophoretic velocities. Disregarding rotational movements of the bead and hydrodynamic interactions, we suggest that (i) Faxen law²⁵ describes the hydrodynamic component of the effective speed, and (ii) a flat velocity profile along the vertical axis can be used to model electrophoresis (see Methods section). Finally we compute the flow around one particle placed in hydrodynamic or electrohydrodynamic flow fields by solving 2D creeping flow equations with finite element methods (lower panel in Figure 1B). Upon application of an electric field, the shear rate at the vicinity of the bead is enhanced near the centerline or near the wall (upper panel of Figure 1B) depending on whether the particle is slowed down or accelerated (blue and green datasets), respectively. Consequently, the amplitude of the electric field modulates the shear around the particle, and so the transverse viscoelastic force. We therefore suggest that the application of an electric field allows us to control the direction and the amplitude of cross stream forces in viscoelastic fluids.

Cross stream forces acting on nanoparticles

We decided to characterize the transport of 200 nm particles conveyed in rectangular channels of $h=7\ \mu\text{m}$ in height and $w=300\ \mu\text{m}$ in width filled with a 2% PVP solution. We used wide field velocimetry, and extracted the longitudinal velocity distribution (Figure 1C). The pressure drop was set so that the peak of the velocity distribution was at $\sim 100\ \mu\text{m/s}$ (green dataset in Figure 1C), and the corresponding average speed was $83\ \mu\text{m/s}$. The negative charge of the tracers, which is characterized by a surface potential of $-41\pm 2\ \text{mV}$ (Malvern ZetaSizer), allowed us to combine electrophoresis and hydrodynamics. The electric field was first adjusted to force particle migration at $30\ \mu\text{m/s}$ in the opposite direction to the flow (purple dataset in the inset of Figure 1C), and the two fields were then actuated simultaneously. The shape of the resulting velocity distribution was flattened (purple dataset in Figure 1C), and the average speed decreased more rapidly than the linear subtraction of hydrodynamics and electrophoresis from 83 to $43\ \mu\text{m/s}$. Further, as described in ref.²⁶, the analysis of the shape of velocity distributions enabled us to measure the particle distribution across the channel height with no adjustable parameter. Focusing toward the channel centerline occurred without electrophoresis (Figure 1D), in agreement with earlier studies¹⁵, whereas an accumulation of particles towards the walls was detected in the presence of an electric field acting

opposite to the flow. These experiments therefore confirmed that the orientation of cross stream forces could be monitored with combined electrophoretic and counter flow.

We then investigated the size dependence of cross stream forces using tracers of 100 and 300 nm co-flowing in a channel of 2.2 μm in height. The particles were identified according to their relative difference intensity (not shown), and the respective velocity distributions were extracted. Without electrophoresis, both velocity distributions were peaked at 140 $\mu\text{m}/\text{s}$, although that of 300 nm particles was expectedly sharper due to their focusing at the centerline. Given that these tracers have similar surface potentials of -40 ± 2 mV and hence comparable electrophoretic mobilities (not shown), we assayed the effect of electro-hydrodynamic actuation. A narrowly-peaked velocity distribution was obtained for 300 nm particles, whereas that for 100 nm tracers was flat in comparison (Figure 1E). The associated concentration profiles indicated the sharp accumulation of 300 nm particles towards the walls (Figure 1F). In turn this experiment highlighted that the relative difference in velocity between the two types of particles $(v_{300} - v_{100})/v_{300}$ decreased from +18% without electrophoresis to -65% with the electric field, and suggested that the simultaneous use of an electric field and a counter flow offered an efficient strategy for size separation.

Cross stream forces acting on DNA

We subsequently inquired whether cross stream forces could also be observed with DNA molecules. To this aim, we tracked the motion of fluorescently labeled DNA molecules (~ 50 kbp). The velocity distribution was recorded in a 2 μm -thick channel at a constant pressure drop of 10 bar/m and for a range of electric fields spanning 0-2.5 kV/m (Figure 2A). The corresponding mean hydrodynamic velocity was 230 $\mu\text{m}/\text{s}$ (yellow histogram in Figure 2A), and electrophoretic velocity varied from 0 to 60 $\mu\text{m}/\text{s}$, *i.e.* less than 25% of the hydrodynamic flow speed. The consequences of cross stream forces could readily be assessed from the sharp slow down in velocity that was much greater than the linear subtraction of the electrophoretic speed (indicated by colored arrows in Figure 2A). This trend was similarly detected in the plot of DNA average velocity as a function of the electric field (Figure 2B), which showed an initial slope 17 times steeper than expected without coupling between hydrodynamics and electrophoresis (dashed lines). Further we wished to directly demonstrate the preferential localization of DNA near the walls. The electric field was adjusted to reach the stagnation point shown in Figure 2B. We then characterized the vertical position of DNA molecules stopped in the field of view of the microscope by recording a series of stacks separated by 330 nm across a channel of 2 or 12 μm in thickness (Figure 2C). The average intensity distribution for 20 molecules was characterized by a bi-modal shape (graph in Figure 2C), confirming the accumulation of DNA near the walls due to viscoelastic transverse forces. Furthermore we noted that the velocity distribution of molecules close to the walls, *i.e.* in the high electric field regime, was

narrower than in the absence of electric field (light green vs. red histograms in Figure 2A). This effect was qualitatively coherent with the confinement of DNA at the walls. Indeed Taylor dispersion, which defines the diffusivity in pressure-driven flows, is proportional to with $v_0^2 h^2$ divided by the diffusion coefficient²⁷. Confined molecules only explore a fraction of the channel at a reduced velocity, hence the effective height and velocity with transverse viscoelastic forces that are relevant to estimate Taylor dispersion are smaller than h and v_0 . In order to quantitatively characterize the reduction in diffusivity, we normalized the breadth of the velocity distribution along the x axis to that obtained in the y direction (see Figure 1A for geometry), in which Brownian diffusion was only contributing to dispersion. This data shown in the inset of Figure 2B established that the amplitude of fluctuations was reduced by a factor of ~ 7 with electro-hydrodynamic actuation. Hence our technology appeared to overcome the limitation of Taylor dispersion in pressure-driven flows for microfluidic separation, which has so far met limited success without the use of confined channels^{28,29}.

Finally we investigated the potential of electrohydrodynamic flows for size-based separation by assaying the behavior of two DNA species of 48.5 and 5.4 kbp (λ -DNA and ϕ X174, respectively) simultaneously conveyed in a microchannel of 2 μm . We extracted their respective velocity distributions (Supplementary Figure S2), and evaluated the relative difference in speed as a function of the ratio β , which was defined by the electrophoretic velocity divided by the mean flow velocity $2/3v_0$ (Figure 2D). Without electric field, the migration of λ -DNA was expectedly faster than that of ϕ X174 due to the enhancement of viscoelastic focusing toward the channel centerline for high molecular weight molecules, as was reported in ref.¹⁵. Note however that dispersion was maximal, hence separations were unfavorable, in this regime (see more below). With electrophoresis, the orientation of cross stream forces towards the walls changed the migration order. The maximal difference in velocity between λ -DNA and ϕ X174 was $\sim 30\%$ using a low flow velocity of $v_0 \sim 80 \mu\text{m/s}$ (red dataset in Figure 2D), suggesting that actuation parameters could be tuned to enhance the performance of DNA size separation experiments.

DNA size separation

We then focused on DNA separation using three DNA molecular weight (MW) markers conveyed in custom-made microfluidic chips or in capillaries. The main difference between these technologies is associated to the length of the separation channel, which was at least of 12 cm for Agilent Capillary Electrophoresis vs. 0.5 cm for our microfluidic devices. Given the sieving properties of PVP for DNA separation³⁰, we started with conventional electrophoresis carried out in a 10 μm capillary filled with a 2% PVP solution. Most bands of a kb-ladder were resolved in ~ 50 minutes with an electric field of 3 kV/m (left panel of Figure 3A). We then optimized electro-hydrodynamic

actuation parameters in the same capillary (see Supplementary Figure S3 for optimization strategy), and resolved the bands of the separation standard in less than 30 minutes (middle panel of Figure 3A). The resolution of the separation in viscoelastic fluids between the 0.5 and 10 kb fragments was enhanced, 28.0 using electro-hydrodynamics vs. 17.8 with electrophoresis (see Methods for definition). Further, according to our model of separation based on transverse viscoelastic forces, these experiments could be carried out in channels with minimal confinement, e.g. in a capillary of inner diameter $D \sim 75 \mu\text{m}$. Indeed the bands comprised between 1 and 48.5 kbp were resolved in less than 17 minutes with electro-hydrodynamic actuation (right panel of Figure 3A). This time to result compares well with the run time of 3 hours in slab gels, as reported by the supplier for this MW marker. Conversely high-performance capillary electrophoresis using polymer blends as separation matrix allows one to reach time to result of 2 minutes for DNA molecules in the size range 0.2-20 kbp³¹.

We subsequently investigated the separation mechanism in microfluidic chips of $2 \mu\text{m}$ in thickness. The pressure was set at 10, 25, and 150 bar/m in order to resolve DNA bands in the range 0.5-10 kb (Figure 3B). Optimal results were obtained for a mean flow velocity of $220 \mu\text{m/s}$ and an electrophoretic speed of $45 \mu\text{m/s}$, allowing us to complete the separation in ~ 7 minutes (middle panel of Figure 3B). Furthermore the modulation of the flow rate towards high or low velocities enabled us to improve the resolution of the separation for high or low molecular weight (MW) molecules, respectively (right and left panels of Figure 3B). Using a low flow rate (purple curve, right panel in Figure 3B), the cross flow migration force was insufficient to modulate the velocity of molecules shorter than $\sim 2 \text{ kb}$, which reached the detector in a single peak characterized by a speed roughly equal to the linear combination of hydrodynamics and electrophoresis (not shown). In order to recapitulate the three experiments in Figure 3B, we computed the ratio of DNA speed to the mean flow velocity as a function of MW (Figure 3C). For each condition, we observed a monotonic decrease in DNA speed, which was associated to the onset of transverse forces with DNA size. The three curves also exhibited a sharp velocity decrease in a size range that could be tuned by adjusting the pressure drop and the electric field. Hence, the modulation of transverse forces in electro-hydrodynamic separation provided an efficient solution for DNA size analysis. Furthermore we checked that transverse forces were predominantly determined by the shear rate by plotting the results obtained in $10 \mu\text{m}$ capillaries (middle panel of Figure 3A) at the same shear rate of $\sim 110 \text{ s}^{-1}$, which were nearly coincident with the data obtained in microfluidic chips (dashed and black curves in Figure 3C). Altogether this set of data confirmed the relevance of electro-hydrodynamic actuation for DNA separation in the size range 0.5-50 kbp.

Finally we evaluated the performance of our separation strategy by plotting (i) DNA velocity and (ii) the theoretical plate number per meter N^{32} as a function of MW (see Methods for definition,

Figure 3D-E). The first plot showed the weak variation of DNA electrophoretic mobility (red dataset in Figure 3D) in comparison to the responses obtained with electro-hydrodynamic actuation. The typical scaling exponent of ~ -2 (dashed line) was in fact much more favorable for separation than that of conventional electrophoresis of -1 ¹. In turn this result explained that the bands of a kb ladder could be resolved in a chip with a separation channel of only 0.5 cm. We subsequently estimated N , which spanned 10^3 - 7.10^5 and appeared to be slightly smaller than with electrophoresis (red dataset in Figure 3E). Optimal results of $N \sim 2.10^6$ obtained with electrophoresis in Lab-on-Chips^{30,33} confirmed this trend that the peaks of our separations were broader for a given separation time than those obtained with electrophoresis. We explained this result by the residual band broadening associated to Taylor dispersion near the walls of electro-hydrodynamic actuation (see e.g. inset of Figure 2B). Notably this interpretation was supported by the low values of N obtained in capillaries (lower blue dataset in Figure 3E): the overly long separation channel was associated to prolonged run times, hence with more dispersion of the peaks. Consequently, the key feature of our technology lies in the sharp variations of DNA velocity with its MW, which are partly balanced by band broadening effects associated to hydrodynamic actuation.

Simultaneous separation and enrichment

Finally we hypothesized that electro-hydrodynamic actuation could be used to enrich DNA in a funnel. According to conservation laws, the electric and flow fields increase proportionally in a constriction except at the vicinity of the apex (Figure 4A). In the parameter space (E, v_0) , the trajectory of DNA molecules located at the center of the channel (black arrow in Figure 4A) follows a line starting from low values of (E, v_0) , *i.e.* near the origin (Figure 4B). Using a set of actuation parameters appropriately defined, the migration regime is dominated by hydrodynamics far from the funnel, so that transport ahead of the funnel is oriented towards this structure. As the molecule progresses toward the apex, the flow velocity increases and transverse viscoelastic forces build-up, leading to the progressive decrease of its effective velocity until it reaches the stagnation point where electrophoretic and hydrodynamic forces balance (red circle in Figure 4B). Past this position, conversely, DNA transport is forced by electrophoresis and oriented backwards to the stagnation point, therefore defining a region in which DNA enrichment occurs. Moreover the enhancement of viscoelastic forces with DNA MW is expected to lead to size dependent stagnation positions (Supplementary Fig. S4A), allowing us to perform separation and enrichment operations simultaneously. Note that this approach is reminiscent of several technologies with electric fields and counter flows, yet all developed with Newtonian fluids so that electric fields at least 10 times greater are necessary (Supplementary Fig. S4B). First DNA concentration has been achieved by flowing a sample in a capillary tube, in which electrodes are incorporated by gap junctions³⁴⁻³⁶. DNA molecules

are stalled by electrophoresis in between the gap junctions. In another direction electro-osmotic flows in balance with counter hydrodynamic flows have been exploited to enrich (i) DNA in a capillary filled with gradient concentration of polymers³⁷ or (ii) microparticles in a microfluidic chip with a constriction³⁸.

To validate this hypothesis, we conveyed the 100 bp ladder in a funnel of 2 μm in thickness. An onset in fluorescence intensity was detected after 30 seconds (Figure 4C), and three bands could be isolated together with a broad unresolved pattern at the constriction. Assigning the pressure drop and the electric field to lower or higher intensities allowed us to resolve 2 or 5 bands, respectively (left and middle panel of Figure 4D, Supplementary video S1). Given that the conditions to reach the stagnation position require increasingly high electric and pressure fields for low MW molecules (Supplementary Figure S4A), we concluded that the high molecular weight bands of 1500, 1000 and 800 bp were resolved in Figure 4C. In order to detect 8 bands out of 9 of the 100 bp ladder, we used a shallower funnel of 1 μm and higher PVP concentrations of 4% with 7 bars of pressure difference (right panel of Figure 4D). Size separation was achieved in ~ 30 s (Supplementary video S2) and DNA enrichment by a factor of ~ 50 per minute was detected for the 300 bp lane for an initial DNA concentration of 0.03 ng/ μL (Supplementary Figure S4C). Focusing on enrichment kinetics, we measured the total fluorescence over time for the bands of 1500, 1000 and 800 bp highlighted in Figure 4C, and deduced that the enrichment rate of 12-, 30-, and 42-fold per minute (left panel of Figure 4E) was uncorrelated with the concentration of each lane of 13.5, 16.5, and 25 ng/ μL , respectively. We suggest that this discrepancy was associated to the difference in effective velocity between the different DNA species during their transport ahead of the constriction. Bearing in mind that the concentration factor was size dependent, we focused on the optimization of this parameter by tuning the pressure and the electric field (right panel of Figure 4E) and reached enrichment rates of 10^3 per minute (Supplementary Figure S4D). We wished to compare these results to those obtained with electrokinetic trapping, in which electroosmosis and electrophoresis act in opposition for DNA concentration^{39,40}, or with dielectrophoretic trapping of molecules in electric field gradients^{41,42}. While enrichment factors of 60-fold per minute have been achieved with the former method, state-of-the-art concentration rates of more than 10^5 per minute were reported in nanofabricated structures⁴¹. Therefore, our technology, which, to the best of our knowledge, has a unique potential for simultaneous separation and concentration operations, compares favorably with electrokinetic trapping, but does not compete with the performances of dielectrophoresis. However, this disadvantage is compensated for by the simplicity of the fabrication process that only involves one step of photolithography. Altogether, we have demonstrated that electro-hydrodynamic actuation offers unique perspectives to simultaneously complete the operations of DNA enrichment and separation on a chip.

Conclusion

We have established the conditions for DNA separation and enrichment in electro-hydrodynamic bi-directional viscoelastic flows. Transverse forces oriented towards the walls constitute the driving mechanism of DNA manipulation. Our strategy therefore appears to be reminiscent of field-flow fractionation (FFF) techniques, in which separation in a Poiseuille flow is achieved through cross stream forces⁴³. In contrast to FFF, however, transverse forces are induced by co-linear hydrodynamic and electric fields, and their amplitude can readily be monitored with conventional fluidic actuation technologies. In addition the viscoelastic solution, which is composed of the cheap, biocompatible, and broadly accessible synthetic polymer PVP, is characterized by a moderate viscosity that is compatible with fluid manipulation in Lab-on-Chips. Our technology hence presents an opportunity for a variety of developments in genomic analysis in miniaturized systems. Future improvements of separation and/or enrichment performances may be achieved by investigating the relationship between the resolution of separations and the fluid viscoelastic properties. Indeed, the fluid characteristics can be monitored by tuning the molecular weight and/or the concentration of dissolved polymers, e.g. PVP or poly-ethyleneoxyde, in order to modulate the amplitude of transverse migration forces. This approach is consistent with the rigorous formulation of the separation matrix with polymer blends for ultrafast separation of long DNA fragments by capillary electrophoresis³¹. More generally, the conception of a model of DNA transport, in which the fluid properties, the geometry of the channel and the actuation parameters are determined for high-performance DNA separation and enrichment, is highly desirable to consolidate our technology. With these guidelines, the separation and enrichment of other biomolecules, such as proteins or RNA strands, may be investigated experimentally in purified conditions, and maybe also in complex media, such as blood or plasma.

Methods

Chemicals and reagents

Molecular biology grades chemicals were purchased from Sigma-Aldrich (France). The buffer for our experiments was TBE 2X (Tris-HCl 160 mM, boric acid 160 mM, EDTA 5 mM, pH = 8.3). Fluorescent nanoparticles were obtained from BangsLabs (Polysciences). Their Zeta potential was measured with the Malvern ZetaSizer. We used four different DNA ladders (Supplementary Figure S3), namely ExactLadder DNA PreMix 100 bp Plus (Ozyme) for enrichment experiments, and 100 bp & 1 kb DNA

ladder (NEB) or 1 kb Extend DNA Ladder (NEB) for size separation, as well as Lambda DNA and the linearized plasmid ϕ X174 supplied from NEB. DNA concentration was set to 10 ng/ μ L in separation experiments, 0.5 ng/ μ L in enrichment experiments, and 0.5 ng/ μ L for single particle tracking. The fluorophore YOYO-1 was purchased from Thermofisher, and used at a (DNA:YOYO-1) staining ratio of 10:1. 2% Dithiothreitol was added to the buffer for single molecule imaging in order to reduce photocleavage.

Imaging set-up and electrophoregrams

Imaging was performed with a Zeiss epifluorescence microscope equipped with the 38HE filter set, and with a Lumencor Light Engine emitting at 475 nm with a bandwidth of 28 nm. For single particle tracking experiments with DNA or nanoparticles at a volume fraction of 10^{-5} , we used a 100X or 20X objective with numerical apertures of 1.4 and 0.75, respectively. An ANDOR iXon-885 camera was used with a binning of 2×2 . Pressure was monitored with a MFCS controller (Fluigent, Paris) delivering up to 1 or 7 bars, and electric fields were controlled with 300 V DC supplier. Capillary electrophoresis was carried out with 7100 Capillary Electrophoresis system (Germany) equipped with a Zetalif LED 480nm detector (Picometrics Technologies, France). Capillaries of different diameters were purchased from Polymicro Technologies (Phoenix, US). YOYO-1 labeled DNA injection (10 ng/ μ L) was carried out during 5 seconds at an electric field of 30 kV/m in the sample reservoir. Electrophoregrams were obtained by recording intensity temporal evolution at a distance of 12 cm from the inlet.

For experiments in microfluidic chips, we recorded time series and analyzed images following two different strategies. On the one hand, DNA or particles were isolated by intensity-based segmentation performed in ImageJ. Trajectories were subsequently reconstructed using Particle Point Analysis in *Matlab* (MATWORKS), and velocity distributions were extracted, as described in ref. ²⁶. In order to monitor the distribution of λ -DNA molecules across the channel height in Figure 2C, we measured the fluorescence intensity of single molecules in the consecutive stacks along the z-direction and then averaged the signal. On the other hand, intensity measurements were carried out to extract electrophoregrams. Enrichment factors (*EF*) for individual bands in the funnel were also computed by measuring the total intensity in one band $I(t)$ at each time point normalized by:

$$EF(t) = \frac{I(t) - I_{BG}}{I_0 - I_{BG}} \quad (1)$$

with I_0 , and I_{BG} the initial intensity of the band and the background signal for buffer flowing in the chip, respectively.

Analysis of separation experiments

The performance of separations was evaluated by measuring the separation time t_{DNA} and the peak width at half maximum w_{DNA} for each peak of electrophoregrams, and we evaluated the theoretical plate number per meter:

$$N = 5.545 \times \left(\frac{t_{DNA}}{w_{DNA}} \right)^2 / l_{sep} \quad (2)$$

with l_{sep} the length of the separation channel. The resolution of the separation between specie 1 and 2 was defined by:

$$Res = \frac{t_{DNA}^1 - t_{DNA}^2}{w_{DNA}^1 + w_{DNA}^2} \quad (3)$$

ODE modeling

Using COMSOL, we solved creeping flow equations in 2D with a particle conveyed by a flow field and an electric field. The bead effective velocity was assumed to be the linear combination of Faxen law and electrophoresis, according to:

$$v(z) = 4v_0 \left\{ \left(\frac{z}{h} \right)^2 - \frac{1}{4} + \frac{1}{3} \left(\frac{a}{h} \right)^2 \right\} - v_E \quad (4)$$

with a the radius of the particle and v_E the electrophoretic velocity.

Acknowledgments: We thank F. Ginot and L. Saias for critical reading of the manuscript, and B. Lonetti for technical help in rheological measurements. H.R. thanks the French ministry of Research for funding. This work was partially funded by Toulouse Tech Transfer program μ LAS, and by the ANR projet JC08_341867. This work was also supported by the LAAS-CNRS technology platform, a member of the French Basic Technology Research Network.

- 1 J. L. Viovy, *Rev Mod Phys*, 2000, **72**, 813–872.
- 2 W. D. Volkmuth and R. H. Austin, *Nature*, 1992, **358**, 600–602.
- 3 K. D. Dorfman, *Rev. Mod. Phys.*, 2010, **82**, 2903–2947.
- 4 N. Kaji, Y. Tezuka, Y. Takamura, M. Ueda, T. Nishimoto, H. Nakanishi, Y. Horiike and Y. Baba, *Anal Chem*, 2004, **76**, 15–22.
- 5 O. Bakajin, T. A. J. Duke, J. Tegenfeldt, C.-F. Chou, S. S. Chan, R. H. Austin and E. C. Cox, *Anal Chem*, 2001, **73**, 6053–6056.
- 6 J. Han and H. G. Craighead, *Science*, 2000, **288**, 1026–1029.
- 7 M. N. Albarghouthi and A. E. Barron, *Electrophoresis*, 2000, **21**, 4096–4111.
- 8 A. T. Woolley and R. A. Mathies, *Anal. Chem.*, 1995, **67**, 3676–3680.
- 9 J. Zheng and E. S. Yeung, *Anal Chem*, 2002, **75**, 3675–3680.
- 10 K. J. Liu, T. D. Rane, Y. Zhang and T.-H. Wang, *JACS*, 2012, **133**, 6898–6901.
- 11 X. Wang, V. Veerappan, C. Cheng, X. Jiang, R. D. Allen, P. K. Dasgupta and S. Liu, *J Am Chem Soc*, 2010, **132**, 40–41.
- 12 R. Tijssen, J. Bos and M. E. Van Kreveld, *Anal. Chem.*, 1986, **58**, 3036–3044.
- 13 A. M. Leshansky, A. Bransky, N. Korin and U. Dinnar, *Phys Rev Lett*, 2007, **98**, 234501.
- 14 F. Del Giudice, G. Romeo, G. D’Avino, F. Greco, P. A. Netti and P. L. Maffettone, *Lab. Chip*, 2013, **13**, 4263.
- 15 K. W. Seo, H. J. Byeon, H. K. Huh and S. J. Lee, *RSC Adv.*, 2014, **4**, 3512–3520.
- 16 G. D’Avino and P. L. Maffettone, *J. Non-Newton. Fluid Mech.*, 2015, **215**, 80–104.
- 17 M. M. Villone, G. D’Avino, M. A. Hulsen, F. Greco and P. L. Maffettone, *J Non-Newton Fluid Mech*, 2013, **195**, 1–8.
- 18 G. Romeo, G. D’Avino, F. Greco, P. A. Netti and P. L. Maffettone, *Lab Chip*, 2013, **13**, 2802–2807.
- 19 E. F. Lee, D. L. Koch and Y. L. Joo, *J. Non-Newton. Fluid Mech.*, 2010, **165**, 1309–1327.
- 20 D. Milanova, R. D. Chambers, S. S. Bahga and J. G. Santiago, *ELECTROPHORESIS*, 2012, **33**, 3259–3262.
- 21 P. Knappe, R. Bienert, S. Weidner and A. F. Thünemann, *Polymer*, 2010, **51**, 1723–1727.
- 22 G. D’Avino, G. Romeo, M. M. Villone, F. Greco, P. A. Netti and P. L. Maffettone, *Lab Chip*, 2012, **12**, 1638–1645.
- 23 Y. Viero, Q. He, L. Mazenq, H. Ranchon, J. Y. Fourniols and A. Bancaud, *Microfluid. Nanofluidics*, 2012, **12**, 465–473.
- 24 R. B. Bird and J. M. Wiest, *Annu. Rev. Fluid Mech.*, 1995, **27**, 169–193.
- 25 J. Happel and H. Brenner, *Low Reynolds Number Hydrodynamics: with Special Applications to Particulate Media*, Kluwer, The Hague, 1983.
- 26 H. Ranchon, V. Picot and A. Bancaud, *Sci. Rep.*, 2015, **5**, 10128.
- 27 G. I. Taylor, *Proc R Soc Lond.*, 1953, **A219**, 186–203.
- 28 D. Stein, F. H. J. van der Heyden, W. J. A. Koopmans and C. Dekker, *Proc Natl Acad Sci USA*, 2006, **103**, 15853–15858.
- 29 X. Wang, L. Liu, G. Guo, W. Wang, S. Liu, Q. Pu and P. K. Dasgupta, *TrAC Trends Anal. Chem.*, 2012, **35**, 122–134.
- 30 Q. Gao and E. S. Yeung, *Anal. Chem.*, 1998, **70**, 1382–1388.
- 31 M. Sun, J. S. Lin and A. E. Barron, *Electrophoresis*, 2011, **32**, 3233–3240.
- 32 L. S. Ettre, *Pure Appl. Chem.*, 1993, **65**.
- 33 S. Rahong, T. Yasui, T. Yanagida, K. Nagashima, M. Kanai, G. Meng, Y. He, F. Zhuge, N. Kaji, T. Kawai and Y. Baba, *Sci. Rep.*, 2015, **5**, 10584.
- 34 J. Astorga-Wells, S. Vollmer, T. Bergman and H. Jörnvall, *Anal. Chem.*, 2007, **79**, 1057–1063.
- 35 J. Astorga-Wells, S. Vollmer, S. Tryggvason, T. Bergman and H. Jörnvall, *Anal. Chem.*, 2005, **77**, 7131–7136.
- 36 S.-R. Park and H. Swerdlow, *Anal. Chem.*, 2003, **75**, 4467–4474.
- 37 I.-T. Kuo, T.-C. Chiu and H.-T. Chang, *ELECTROPHORESIS*, 2003, **24**, 3339–3347.
- 38 G.-L. Lettieri, A. Dodge, G. Boer, N. F. de Rooij and E. Verpoorte, *Lab. Chip*, 2003, **3**, 34–39.
- 39 J. Dai, T. Ito, L. Sun and R. M. Crooks, *J. Am. Chem. Soc.*, 2003, **125**, 13026–13027.

- 40 D. Stein, Z. Deurvorst, F. H. J. van der Heyden, W. J. A. Koopmans, A. Gabel and C. Dekker, *Nano Lett.*, 2010, **10**, 765–772.
- 41 K.-T. Liao and C.-F. Chou, *J. Am. Chem. Soc.*, 2012, **134**, 8742–8745.
- 42 C.-F. Chou, J. O. Tegenfeldt, O. Bakajin, S. S. Chan, E. C. Cox, N. Darnton, T. Duke and R. H. Austin, *Biophys. J.*, 2002, **83**, 2170–2179.
- 43 J. C. Giddings, F. J. Yang and M. N. Myers, *Science*, 1976, **193**, 1244–1245.

Figure 1: Transverse migration of nanoparticles in viscoelastic fluids. (A) Representation of the experiment, in which DNA transport is simultaneously actuated with hydrodynamics and electrophoresis. (B) In the lower panel, the plot represents the flow field around a 100 nm particle transported by a Poiseuille flow of maximum velocity $v_0=100 \mu\text{m/s}$ in a $4 \mu\text{m}$ -thick channel (black dataset obtained from finite element modeling). The particle represented by a circle is placed at an arbitrary position midway through the wall and the centerline. Upon application of an electric field that conveys the particle at $\pm 20 \mu\text{m/s}$, the shear stress around the particle is enhanced on the side facing the wall or the centerline, depending on whether the particle is accelerated or slowed down (upper panel). (C) The three histograms represent the velocity distribution of 200 nm tracers transported in $7 \mu\text{m}$ -thick channels with hydrodynamic (green dataset) or electro-hydrodynamic actuation (cyan and purple datasets). The corresponding histograms in the inset represent the velocity distributions for electrophoretically-driven nanoparticles. Note that the Gaussian shape of the distributions with electrophoresis vs. the skewed curve detected for electro-hydrodynamics. (D) The three curves represent the spatial distribution of tracers across the channel height for the same conditions as in panel (C). (E) The graph shows the behavior of 100 nm and 300 nm tracers (smooth or cityscape plots, respectively) transported in microchannels of $2.2 \mu\text{m}$ in height with hydrodynamics or electrohydrodynamics (black and green datasets, respectively). (F) The spatial distribution of tracers across the channel height indicates the stronger accumulation of 300 nm beads towards the walls for the same set of actuation parameters.

Figure 2: Transverse migration of DNA in viscoelastic fluids. (A) In the left panel, the graph shows the velocity distributions obtained for λ -DNA molecules flowing in $2 \mu\text{m}$ -thick microchannels for a constant pressure drop and electric fields of variable amplitudes. The electrophoretic mobility is represented by the set of arrows in the inset. (B) The plot represents the average velocity of λ -DNA as a function of the electric field. The stagnation point corresponds to the conditions in which hydrodynamic and electrophoretic forces are in balance and the velocity of the molecules is null. The lower and upper dashed lines correspond to the initial variation in velocity vs. that expected for a constant hydrodynamic transport and an electrophoretic mobility of $2.5 \cdot 10^{-4} \text{ cm}^2/\text{V.s}$, respectively. The inset shows the ratio of the standard deviation of the velocity distribution in the longitudinal vs. lateral direction as a function of the electric field. (C) In a chip of $12 \mu\text{m}$ in height, the position of λ -DNA molecules arrested in the field of view of the objective is measured using a series of stacks (3 representative images are shown at the top). The graph below represents the average intensity distribution for 20 molecules, which appear to be predominantly located at the walls of the channel.

(D) The relative velocity difference between λ -DNA and ϕ X174 molecules, as inferred from single particle tracking, is plotted as a function of the electric field normalized to the mean flow velocity.

Figure 3: DNA separation using electro-hydrodynamic actuation. **(A)** The curves in the left and in the middle report electrophoregrams obtained for the separation of a kb-ladder by electrophoresis alone or electrohydrodynamic actuation, respectively, using capillary electrophoresis in 10 μm tubings. The electrophoregram in the right shows the separation of kb-extend DNA ladder by electrohydrodynamic actuation in 75 μm capillary. **(B)** The three graphs show electrophoregrams recorded in 2 μm -thick microchannels under different actuation conditions, as indicated in inset. Note that the curve in the left is obtained with the 100-bp ladder and the others with the kb-ladder. **(C)** The plot represents DNA velocity normalized to the maximum flow velocity v_0 of 0.9, 0.22, and 0.58 mm/s as a function of DNA MW (purple, black, and green datasets, respectively). Note the correspondence of the colors with the electrophoregrams in **(B)**. The dashed curve corresponds to the result of capillary electrophoresis (graph in the middle of **(A)**). **(D)** The graph recapitulates the variation of the velocity as a function of MW for all the electrophoregrams shown in **(A)** and **(B)**. **(E)** The theoretical plate number per meter is reported as a function of DNA MW for different experimental conditions, namely electrophoresis (red curve), electrohydrodynamic actuation in chips or capillaries (dashed and blue curves, respectively).

Figure 4: DNA enrichment and separation in a funnel. **(A)** In the left panel, the amplitude of the electric and flow fields are predicted by 3D finite element modeling (upper and lower graphs). The electron micrograph in the right represents the funnel just before sealing **(B)** The graph depicts our strategy for a molecule transported along a streamline in the middle of the channel (fire colored line in **(A)**). Starting from low electric and flow fields, the molecule travels to regions where mechanical constraints are high, as indicated by the arrow, until its velocity becomes null (circle). **(C)** The time series shows DNA enrichment and band formation in a funnel for a set of values in pressure and electrophoretic forces. **(D)** The four micrographs correspond to the result of enrichment experiments after 30 seconds for different actuation parameters indicated in the inset. The channel depth is 2 μm for the three images at the left and 1 μm for the micrograph in the right. **(E)** The plots represent the build-up in intensity over time for different bands and a given set of actuation parameters, or the same band with different actuation parameters (left or right panel, respectively). Note that the signal decreases to zero as soon as the electric field is stopped, as shown by the sudden drop in intensity after 40 s in the right panel.

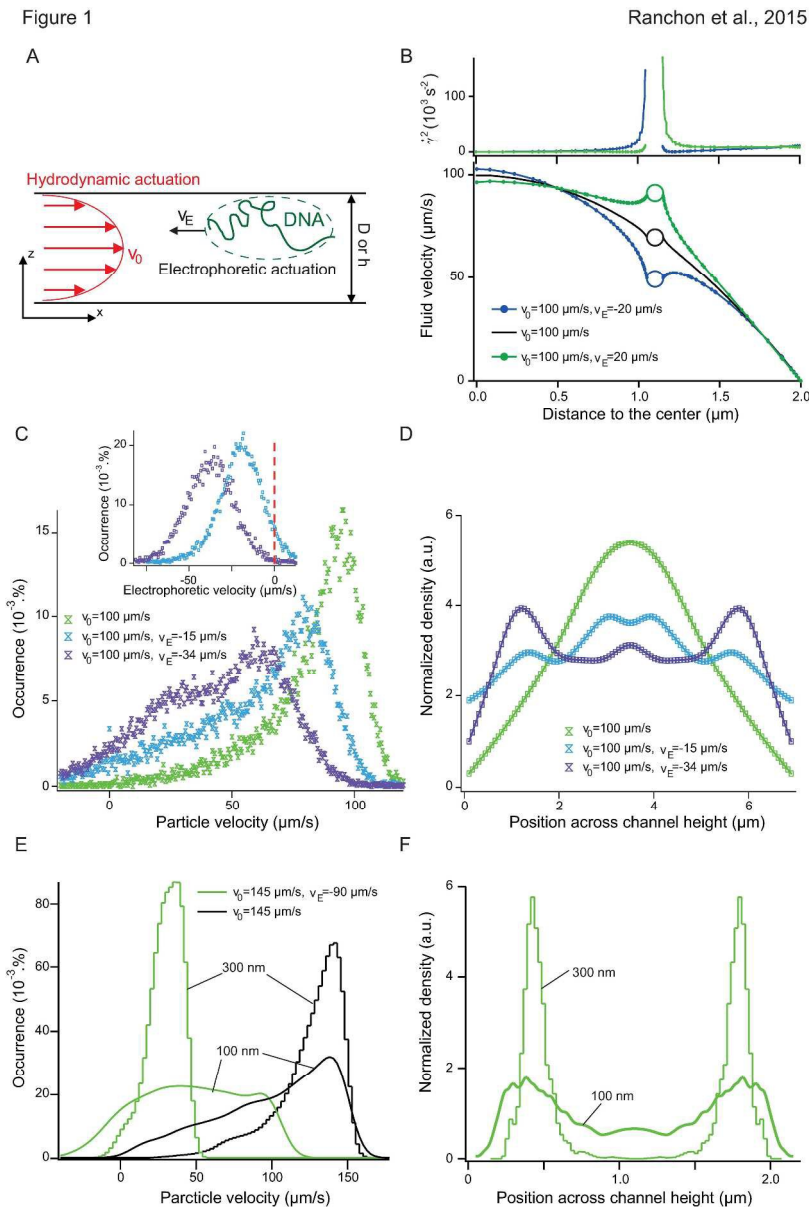


Figure 1: Transverse migration of nanoparticles in viscoelastic fluids. (A) Representation of the experiment, in which DNA transport is simultaneously actuated with hydrodynamics and electrophoresis. (B) In the lower panel, the plot represents the flow field around a 100 nm particle transported by a Poiseuille flow of maximum velocity $v_0=100 \mu\text{m/s}$ in a $4 \mu\text{m}$ -thick channel (black dataset obtained from finite element modeling). The particle represented by a circle is placed at an arbitrary position midway through the wall and the centerline. Upon application of an electric field that conveys the particle at $\pm 20 \mu\text{m/s}$, the shear stress around the particle is enhanced on the side facing the wall or the centerline, depending on whether the particle is accelerated or slowed down (upper panel). (C) The three histograms represent the velocity distribution of 200 nm tracers transported in $7 \mu\text{m}$ -thick channels with hydrodynamic (green dataset) or electro-hydrodynamic actuation (cyan and purple datasets). The corresponding histograms in the inset represent the velocity distributions for electrophoretically-driven nanoparticles. Note that the Gaussian shape of the distributions with electrophoresis vs. the skewed curve detected for electro-hydrodynamics. (D) The three curves represent the spatial distribution of tracers across the channel height for the same

conditions as in panel (C). (E) The graph shows the behavior of 100 nm and 300 nm tracers (smooth or cityscape plots, respectively) transported in microchannels of 2.2 μm in height with hydrodynamics or electrohydrodynamics (black and green datasets, respectively). (F) The spatial distribution of tracers across the channel height indicates the stronger accumulation of 300 nm beads towards the walls for the same set of actuation parameters.

260x388mm (300 x 300 DPI)

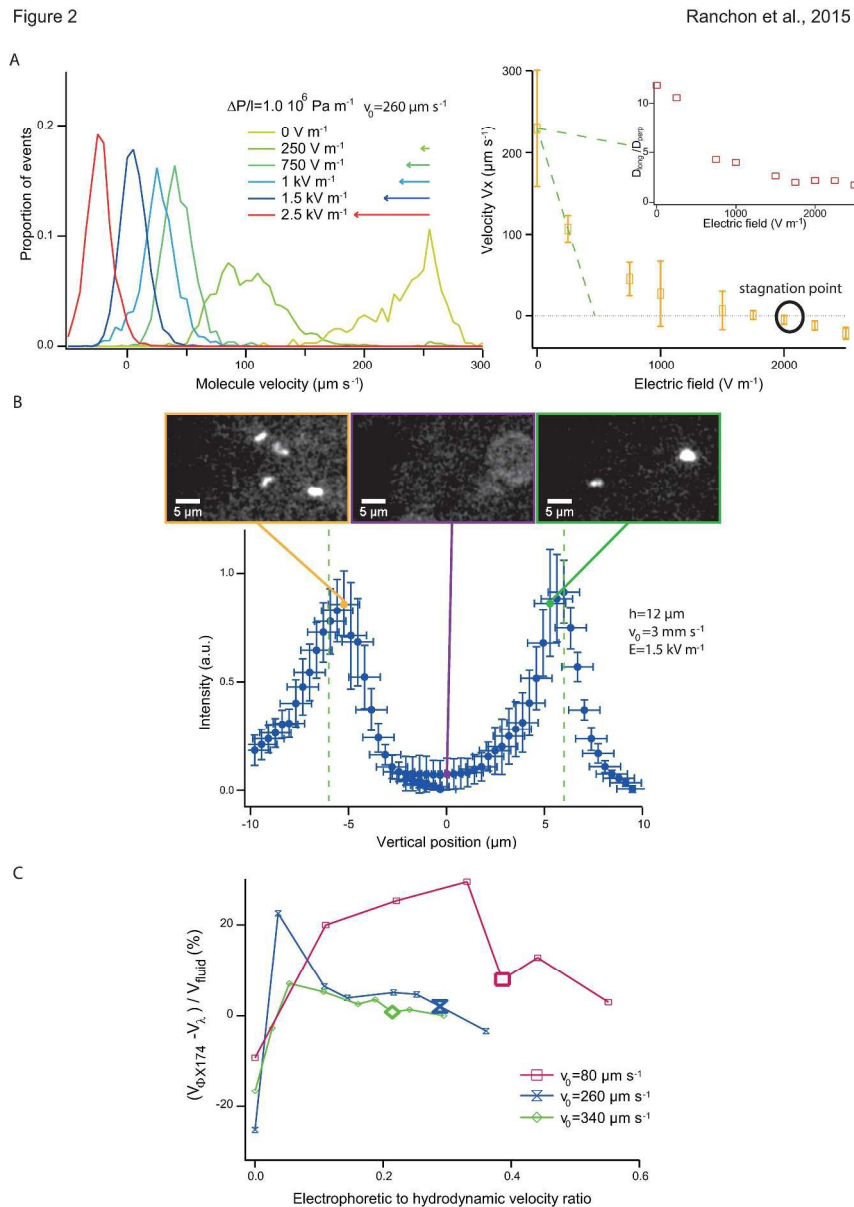


Figure 2: Transverse migration of DNA in viscoelastic fluids. (A) In the left panel, the graph shows the velocity distributions obtained for λ -DNA molecules flowing in 2 μm -thick microchannels for a constant pressure drop and electric fields of variable amplitudes. The electrophoretic mobility is represented by the set of arrows in the inset. (B) The plot represents the average velocity of λ -DNA as a function of the electric field. The stagnation point corresponds to the conditions in which hydrodynamic and electrophoretic forces are in balance and the velocity of the molecules is null. The lower and upper dashed lines correspond to the initial variation in velocity vs. that expected for a constant hydrodynamic transport and an electrophoretic mobility of $2.5 \cdot 10^{-4} \text{ cm}^2/\text{V.s}$, respectively. The inset shows the ratio of the standard deviation of the velocity distribution in the longitudinal vs. lateral direction as a function of the electric field. (C) In a chip of 12 μm in height, the position of λ -DNA molecules arrested in the field of view of the objective is measured using a series of stacks (3 representative images are shown at the top). The graph below represents the average intensity distribution for 20 molecules, which appear to be predominantly located at the walls of the channel. (D) The relative velocity difference between λ -DNA and ϕX174 molecules, as inferred from single

particle tracking, is plotted as a function of the electric field normalized to the mean flow velocity.
284x401mm (300 x 300 DPI)

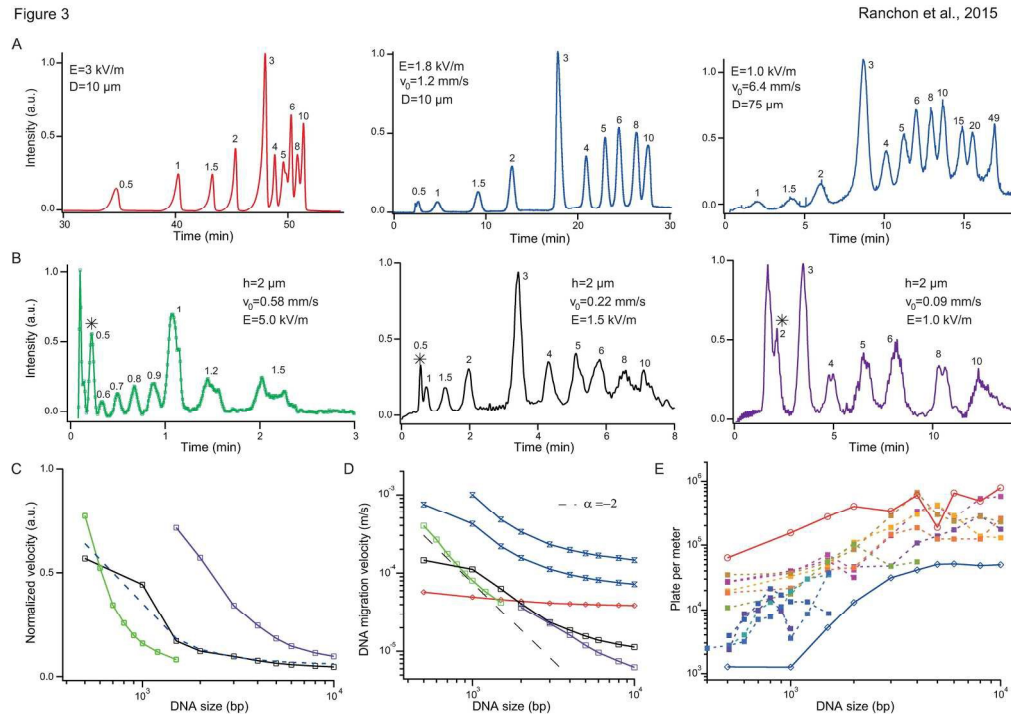


Figure 3: DNA separation using electro-hydrodynamic actuation. (A) The curves in the left and in the middle report electropherograms obtained for the separation of a kb-ladder by electrophoresis alone or electrohydrodynamic actuation, respectively, using capillary electrophoresis in 10 μm tubings. The electropherogram in the right shows the separation of kb-extend DNA ladder by electrohydrodynamic actuation in 75 μm capillary. (B) The three graphs show electropherograms recorded in 2 μm -thick microchannels under different actuation conditions, as indicated in inset. Note that the curve in the left is obtained with the 100-bp ladder and the others with the kb-ladder. (C) The plot represents DNA velocity normalized to the maximum flow velocity v_0 of 0.9, 0.22, and 0.58 mm/s as a function of DNA MW (purple, black, and green datasets, respectively). Note the correspondence of the colors with the electropherograms in (B). The dashed curve corresponds to the result of capillary electrophoresis (graph in the middle of (A)). (D) The graph recapitulates the variation of the velocity as a function of MW for all the electropherograms shown in (A) and (B). (E) The theoretical plate number per meter is reported as a function of DNA MW for different experimental conditions, namely electrophoresis (red curve), electrohydrodynamic actuation in chips or capillaries (dashed and blue curves, respectively).

198x141mm (300 x 300 DPI)

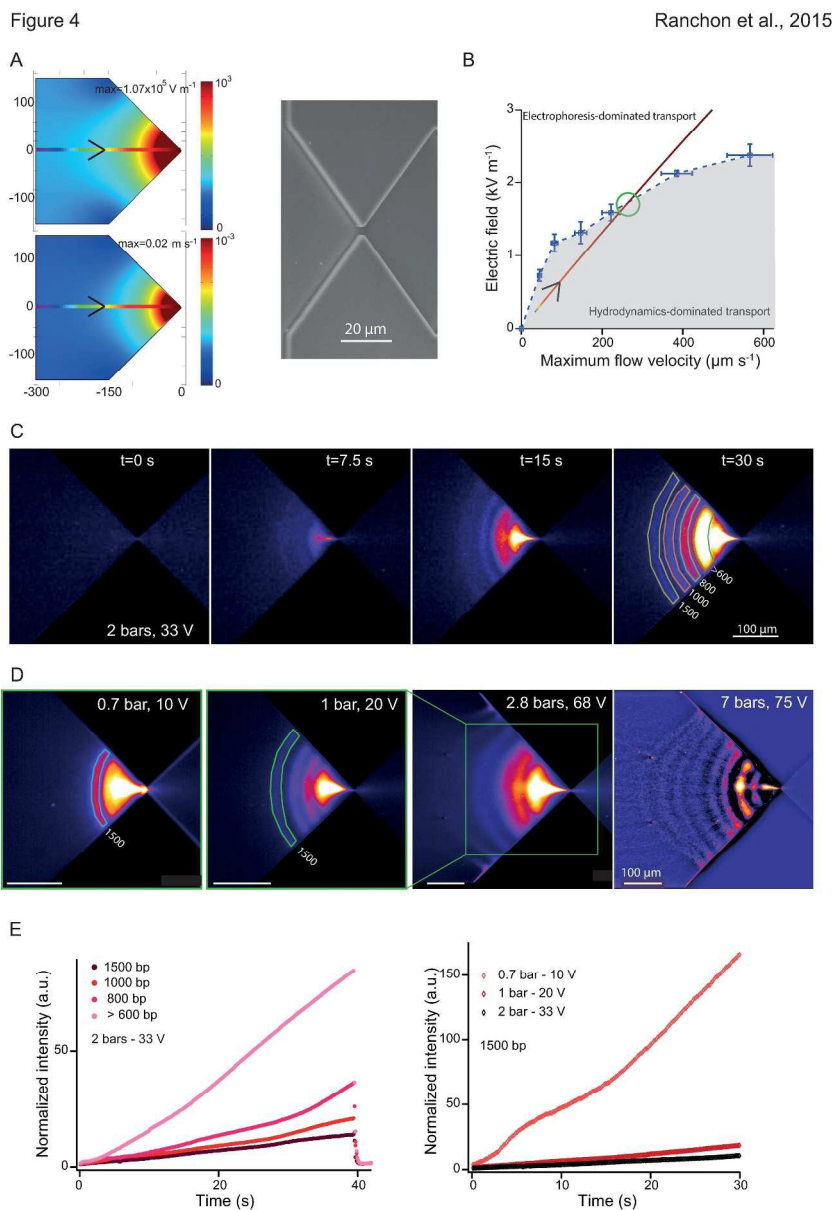


Figure 4: DNA enrichment and separation in a funnel. (A) In the left panel, the amplitude of the electric and flow fields are predicted by 3D finite element modeling (upper and lower graphs). The electron micrograph in the right represents the funnel just before sealing (B) The graph depicts our strategy for a molecule transported along a streamline in the middle of the channel (fire colored line in (A)). Starting from low electric and flow fields, the molecule travels to regions where mechanical constraints are high, as indicated by the arrow, until its velocity becomes null (circle). (C) The time series shows DNA enrichment and band formation in a funnel for a set of values in pressure and electrophoretic forces. (D) The four micrographs correspond to the result of enrichment experiments after 30 seconds for different actuation parameters indicated in the inset. The channel depth is 2 μm for the three images at the left and 1 μm for the micrograph in the right. (E) The plots represent the build-up in intensity over time for different bands and a given set of actuation parameters, or the same band with different actuation parameters (left or right panel, respectively). Note that the signal decreases to zero as soon as the electric field is stopped, as shown by the sudden drop in intensity after 40 s in the right panel.

263x379mm (300 x 300 DPI)